Exp Physiol 94.5 pp 578–596

Experimental Physiology – *Review Article*

Experimental Physiology

Computational cardiac atlases: from patient to population and back

Alistair A. Young[1] and Alejandro F. Frangi[2,3,4]

[1] *Department of Anatomy with Radiology, University of Auckland, Auckland, New Zealand*
[2] *CISTIB, Department of Information and Communication Technologies, Universitat Pompeu Fabra University, Barcelona, Spain*
[3] *Networking Center on Biomedical Research – Bioengineering, Biomaterials and Nanomedicine (CIBER-BBN), Barcelona, Spain*
[4] *Institució Catalana de Reserca i Estudis Avançats, Barcelona, Spain*

Integrative models of cardiac physiology are important for understanding disease and planning intervention. Multimodal cardiovascular imaging plays an important role in defining the computational domain, the boundary/initial conditions, and tissue function and properties. Computational models can then be personalized through information derived from *in vivo* and, when possible, non-invasive images. Efforts are now established to provide Web-accessible structural and functional atlases of the normal and pathological heart for clinical, research and educational purposes. Efficient and robust statistical representations of cardiac morphology and morphodynamics can thereby be obtained, enabling quantitative analysis of images based on such representations. Statistical models of shape and appearance can be built automatically from large populations of image datasets by minimizing manual intervention and data collection. These methods facilitate statistical analysis of regional heart shape and wall motion characteristics across population groups, via the application of parametric mathematical modelling tools. These parametric modelling tools and associated ontological schema also facilitate data fusion between different imaging protocols and modalities as well as other data sources. Statistical priors can also be used to support cardiac image analysis with applications to advanced quantification and subject-specific simulations of computational physiology.

(Received 12 October 2008; accepted after revision 17 December 2008; first published online 19 December 2008)
Corresponding author A. A. Young: Department of Anatomy with Radiology, University of Auckland, Private Bag 92019, Auckland Mail Centre, Auckland 1142, New Zealand. Email: a.young@auckland.ac.nz

A major strategy of Cardiac Physiome projects is to develop mathematical and computer models to integrate the observations from many laboratories into quantitative, self-consistent and comprehensive descriptions (http://www.physiome.org.nz). Many groups have begun to construct physiological databases, linked with anatomical, functional and clinical data gleaned from a variety of sources. This information must be integrated across many scales, from molecular interactions to organ system function. There have been several initiatives begun in this endeavour, centred on different organ systems and pathology targets. Projects include the Integrative Biology Project (http://www.integrativebiology.ox.ac.uk), the ECG signal database (http://www.physionet.org), the Cardiac Gene Expression database (http://www.cage.wbmei.jhu.edu), the Medical Image File Archive Project (http://dpi.radiology.uiowa.edu/mifar/index.php), anatomical ontology databases, such as the Foundational Model of Anatomy (http://sig.biostr.washington.edu/projects/fm/AboutFM.html), and Informatics for Integrating Biology and the Bedside (http://www.i2b2.org/). In particular, the Biomedical Informatics Research Network (http://www.nbrin.net) provides a number of tools to facilitate collaborative research among neuroscientists and medical scientists, making use of computational and networking technologies and addressing issues of user authentication, data integrity, security and data ownership. These tools, and those of the Cancer Biomedical Informatics Grid (https://cabig.nci.nih.gov/) are being exploited by the Cardiovascular Research Grid (http://www.cvrgrid.org) to create an infrastructure for sharing cardiovascular data and data analysis tools. For the brain, the infrastructure for building atlases and computational anatomy tools are well developed. For example, the Center for Computational Biology at UCLA (http://cms.loni.ucla.edu/ccb) provides

DOI: 10.1113/expphysiol.2008.044081

'middleware' applications and software required to provide secure, Web-based access to the underlying computational and network resources, including the International Consortium for Brain Mapping (http://www.loni.ucla.edu/ICBM). At the same time, a number of initiatives worldwide are looking at the research and implementation challenges inherent to all the various organ systems, for example, the IUPS Physiome Project (http://www.physiome.org.nz) and the Virtual Physiological Human European Network of Excellence (http://www.vph-noe.eu).

The vast expansion in the use of the Internet has been instrumental in bringing together a growing number of Physiome centres. These centres provide databases on the functional aspects of biological systems, including the genome, molecular form and kinetics, and cell biology, up to complete functioning organ systems. The databases provide some of the raw information needed to develop models of physiological systems and to simulate whole organs. Data on the physiological functions of cell and tissue structures as well as whole organ systems are growing at dramatic rates, aided by technical advances, such as improved biological imaging techniques. Similarly, modelling resources and software are developing at a rate fast enough to enable the development of realistic computer models of whole organs to commence. At the cellular level, electrophysiological, excitation–contraction coupling, contractile and metabolic processes have been described and modelled mathematically. At the tissue level, the myocardial microstructure and its effects on the mechanical and electrical properties of the heart have been characterized. At the organ level, state-of-the-art finite element analysis methods have been developed to model the complex geometry, non-linear material properties and large deformations of the heart, to enable solution of the biophysical conservation laws linking stress, strain and energy expenditure.

Since multimodal imaging of both structure and function at multiple scales is undoubtedly an excellent technology set for exploring the function of organ systems, the establishment of large imaging databases is essential for the development and validation of these physiological models. Multidimensional image data provide the ability to customize biomechanical and physiological parameters to a particular patient's anatomy and cardiac performance. Large population-based databases also enable statistical models of normal and pathological function to be developed, which in turn facilitates better tools for construction of computational models from image data.

An atlas is an alignment of data maps from different domains, either population (statistically) or individualized (subject specific), which enables querying of relations from multiple domains to construct 'the big picture'. In the brain, for example, atlases have been successfully developed from spatial representations of brain structure and/or function, using registration and warping techniques to align maps between modalities and representations, and relying on indexing schemes and nomenclature systems for standardized classification. Atlases comprised of multiple data sources and many individuals provide the ability to describe shape and functional data with statistical and visual power. A computational cardiac atlas should map the structure and function of the heart across different domains, e.g. different scales of observation, multimodal information sources, across *in silico* and *in vivo* data and/or across patient populations. In this way, computational cardiac atlases integrate huge amounts of otherwise disconnected information to discover the patterns that represent their internal logic or relationships. In this article, we confine ourselves primarily to computational cardiac atlases as a methodology for: (a) analysing anatomical phenotypes across subject populations; (b) performing multimodal image analysis and fusion based on statistical structural constraints for diagnostic or prognostic purposes; and (c) deriving subject-specific physiological models, which could be used to link *in vivo* and *in silico* information about individuals and populations.

Cardiovascular imaging

Many imaging techniques exist to perform cardiovascular examinations (Goldin *et al.* 2000; Reeder *et al.* 2001). Ultrasound (US), single-photon emission computed tomography (SPECT), computed tomography (CT) and magnetic resonance imaging (MRI) are the most well-known and established techniques. However, many recent advances in hardware, contrast agents and postprocessing algorithms are empowering these methods by extending the frontiers of their applicability.

For instance, hardware improvements in MRI, CT and US nowadays allow faster imaging protocols, resulting in (near) real-time dynamic three-dimensional (3-D) imaging of the heart. This has been demonstrated with parallel MRI acquisition strategies (Sodickson & Manning, 1997; Sodickson, 2000; Pruessmann *et al.* 1999; Weiger *et al.* 2000), with multislice CT imaging (Taguchi & Aradate, 1998; Hu, 1999; Klingenbeck-Regn *et al.* 1999, 2002) and with piezoelectric two-dimensional arrays or 3-D probe tracking systems in US (Lees, 2001; Fenster & Downey, 2000; Lange *et al.* 2001).

Cardiac ultrasound still remains the most ubiquitous cardiac imaging modality, with applications at the bedside and during interventions. At the same time, it is the best modality in terms of temporal resolution and the only one able to capture specific features of cardiac dynamics. Albeit with lower temporal resolution, three-dimensional ultrasound has recently received substantial attention in cardiology, particularly in cardiac valve diseases, which require the imaging of valvular dynamics in three dimensions.

Cardiac multidetector computed tomography (MDCT) has established itself as the modality for assessing the structure of the coronary tree *in vivo* with simultaneous acquisition of the dynamic anatomy of the whole heart and great vessels with great spatial detail (0.5 mm isotropic voxels). Unfortunately, this modality still involves substantial radiation, which makes it less suitable when longitudinal or follow-up scans need to be performed.

Cardiac MRI provides an abundant source of detailed, quantitative data on heart structure and function. Advantages of cardiac MRI include its non-invasive nature, well-tolerated and safe (non-ionizing) procedures, ability to modulate contrast in response to several mechanisms, and ability to provide high-quality functional information in any plane and any direction. Its 3-D tomographic nature allows excellent views of the entire heart, irrespective of cardiac orientation and cardiac chamber shape (Fig. 1). Cardiac MRI has provided detailed information on 3-D ventricular shape and geometry (Reichek, 1991; Pattynama *et al.* 1994), regional systolic (Young *et al.* 1994) and diastolic strain (Fonseca *et al.* 2004), material microstructure (Hsu *et al.* 1998; Scollan *et al.* 1998), blood flow (Kilner *et al.* 2000), perfusion (Panting *et al.* 2002) and viability (Kim *et al.* 2000; Wagner *et al.* 2003). It is considered to be the most accurate method for measurement of ventricular volumes and systolic function (Pattynama *et al.* 1994). The high precision and accuracy of cardiac MRI (Myerson *et al.* 2002; Bottini *et al.* 1995) has led to its increasing application worldwide in cardiac research trials and clinical practice.

The Society for Cardiovascular Magnetic Resonance (SCMR) teaching atlas (http://atlas.scmr.org/), created in 1999 and updated in 2007, is an example of a single annotated case and consists of a comprehensive range of cardiac MR images of a healthy volunteer, including cine function images, myocardial tagging images, T1 weighted anatomical images and phase contrast flow images (Fig. 1).

Analysis of shape and motion

Analysis of the ∼500 images which result from a typical functional study has been typically limited to global estimates of mass and volume, and qualitative evaluation of local wall motion. However, these images provide detailed information on regional wall motion during diastole and systole, which can be combined with other imaging or clinical data to yield greater understanding of underlying disease processes.

Model-based analysis tools (Fig. 2) allow the calculation of standard cardiac performance indices, such as left ventricular mass and volume, by efficient customization of a mathematical model to patient images (Young *et al.* 2000). However, they also allow quantitative parameterization of regional heart wall motion, in a way that facilitates statistical comparison of cases drawn from different patient populations (Augenstein & Young, 2001). The mathematical model also provides a mechanism for the integration and comparison of information from different imaging protocols, such as late gadolinium

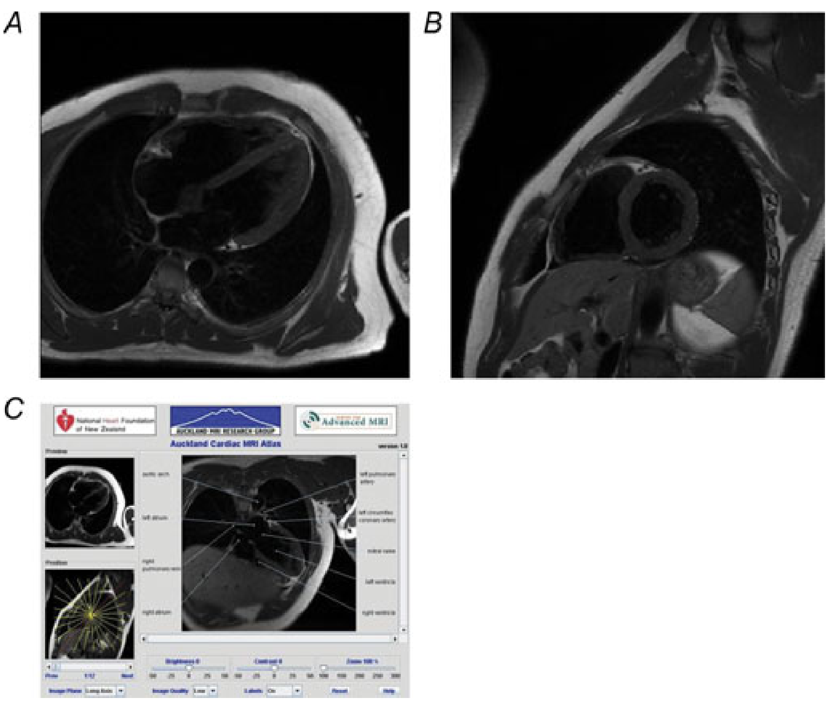

Figure 1. Black blood anatomical images from the SCMR anatomical cardiac magnetic resonance atlas
Image panes are a coronal slice (*A*), a short-axis slice (*B*); and an annotated long-axis slice with applet navigation and viewing tools (*C*; http://atlas.scmr.org/).

enhancement (Oshinski *et al.* 2001; Rehwald *et al.* 2002; Setser *et al.* 2003) and displacement encoding (Young & Axel, 1992; Young *et al.* 1995). For a review of work in this area, see Frangi *et al.* (2005).

In addition to the traditional mass and volume analysis, the mathematical model allows detailed evaluation of regional wall motion and shape characteristics, in relation to a standardized co-ordinate system. Figure 3 shows a bullseye map of regional wall thickness at end-systole, together with plots of wall thickness against time. The software enables users to interactively define a region of interest for wall thickening calculations. Figure 3*B* shows an example of remodelling in infarcted and remote zones in a patient 1 week and 3 months after myocardial infarction.

Another application of the combination of advanced cardiac imaging and statistical anatomical modelling is the evaluation and quantification of asynchronous contraction of the left ventricle (LV) with applications in planning and evaluating pacing treatments, such as cardiac resynchronization therapy (CRT). Figure 4 shows an anatomical model of the heart where the various nodes have been labelled according to the standard bullseye sectorization. Next to it, the time course of wall motion (WM, upper row) and wall thickening (WT, middle row) for the various circumferential sectors are displaced for the basal, medial and apical levels, respectively (in columns). The indices WM and WT attempt to quantify the effect of the passive and active forces acting on the myocardial wall. As shown by this figure, these parameters exhibit a dramatic difference between healthy volunteers and CRT candidates. The lower row shows how it is possible to combine the former indices in a WM *versus* WT plot, which facilitates the integration of the two pieces of information for better discrimination of patients and therefore may aid patient selection for CRT.

Population models

Model-based image analysis procedures provide a powerful mechanism for the fast, accurate assessment of cardiac data and facilitate biophysical analyses and standardized functional mapping procedures. Since the mathematical models employed for motion analysis are registered to the anatomy of the heart, they can be used to derive statistical descriptions of characteristic patterns of regional wall motion in health and disease. This leads to the identification of differences in the characteristic pattern of regional heart wall motion between disease or treatment groups.

However, the differences in regional wall motion parameters between groups are difficult to characterize

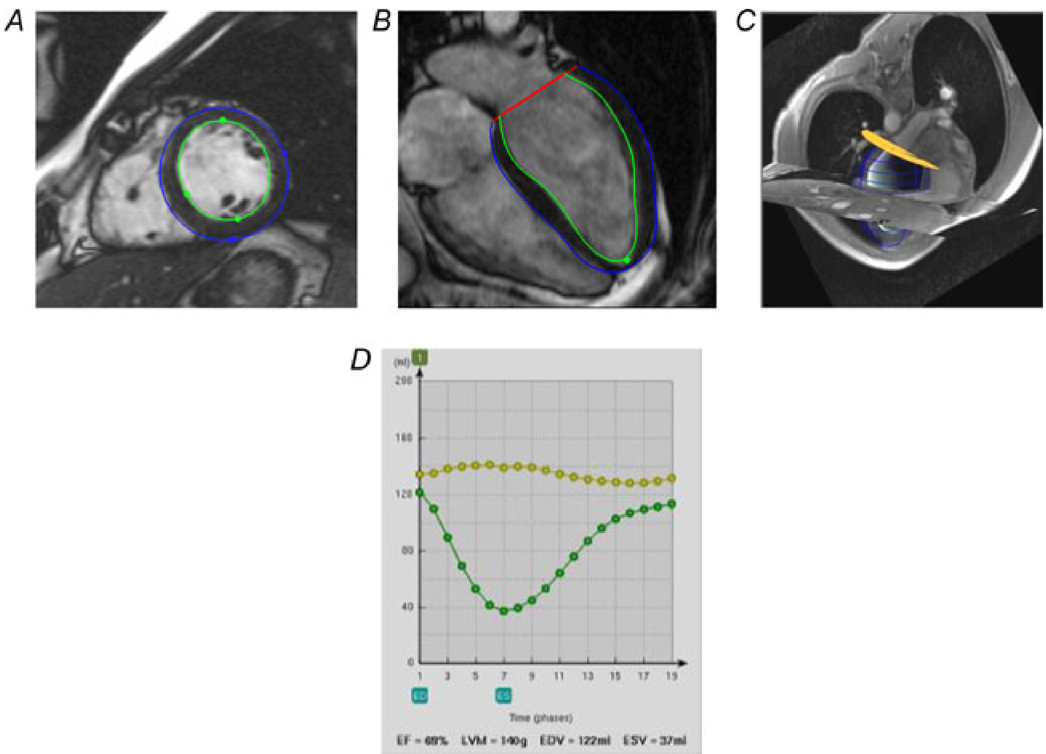

Figure 2. Steady-state free precession cine short- (*A*) and long-axis images (*B*), at end-diastole, with 3-D view of model and images (*C*) and functional data showing LV volume plotted against time (*D*)
Contours show location of the intersection of the 4-dimensional spatio-temporal model with the image plane. Guide points placed by the user are also shown (*A* and *B*; Young *et al.* 2000).

succinctly, owing to their multidimensional nature. Many parameters are required to describe regional performance (including regional strain, rotation and displacement). One powerful technique is principal component analysis (PCA), which describes the major sources of variation within a multidimensional data set by decomposing the variability into a set of orthogonal components or 'modes' (Cootes *et al.* 1994). Thus, a database of models of heart shape and motion can be characterized by a set of orthogonal modes and their associated variance. The modes are ranked in order of highest to lowest variability, thereby showing which variations are most strongly present in the data and which variations can be neglected. This reduces the number of significant parameters by distinguishing the modes that truly differentiate the groups and eliminating modes that are insignificant. Given two such database distributions, describing different patient groups, statistical comparisons can then be made to determine the differences in shape and motion between the two groups. Similarly, given a new case, a comparison could be made with the database distributions to see which database best describes the patient's cardiac performance.

Construction of cardiac atlases, comprising probabilistic maps of heart shape and motion in health and disease, is now an active area of research. Frangi *et al.* (2002) and Lotjonen *et al.* (2004) developed right and left ventricle statistical shape models. Ordas *et al.* (2007) have developed a whole heart computational atlas using registration-based techniques for anatomical correspondence estimation across the population. Perperidis *et al.* (2005) and Hoogendorn *et al.* (2007, 2008) described the construction of a four-dimensional (space and time) probabilistic atlas from cardiac MRI examinations. The information about statistical distributions can then be used to guide image analysis problems, such as segmentation of the heart from MR images, by allowing high-level information on the expected shape and motions of the heart to guide the segmentation problem. For example, Rueckert & Burger (1997) developed a method to maximize the posterior probability of obtaining a model, given an observed data set, based on the prior likelihood of obtaining the model from the historical population and the likelihood of obtaining the data, given the model. van Assen *et al.* (2006), in turn, have used high-level statistical anatomical constraints to recover cardiac models based on a sparse set of image cross-sections. Beg *et al.* (2004) developed a large deformation diffeomorphic metric mapping strategy to build statistical atlases from MRI. To date, although these methods have demonstrated their potential, they have been limited by the relatively small size of the databases available for training, which might therefore bias subsequent image analysis, particularly in pathological situations.

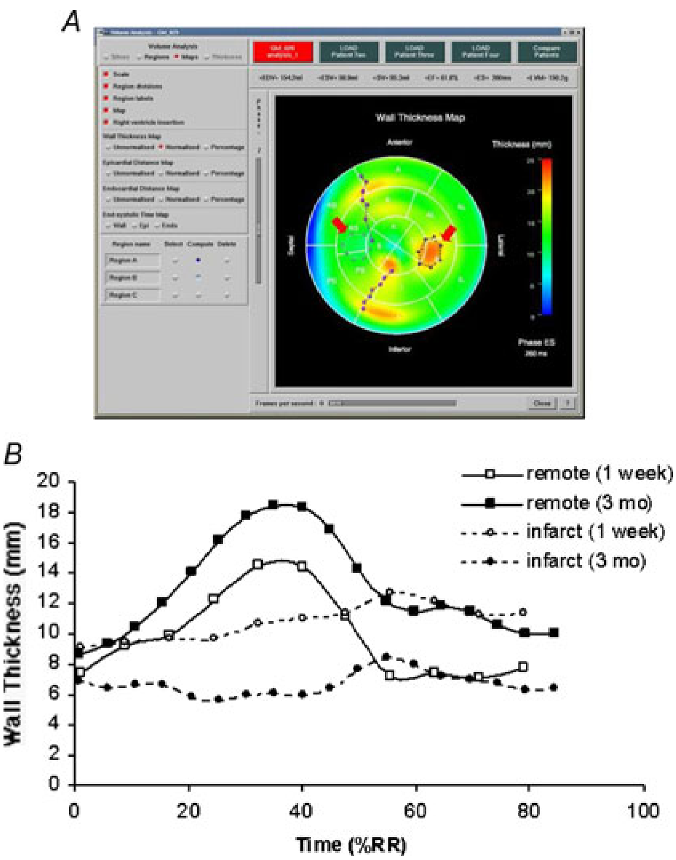

Figure 3. Wall thickness in all regions of the heart can be determined from the mathematical model
A, bullseye plot of wall thickness in each region of the LV, with user-defined regions (arrows) allowing interactive calculation of wall thickness within a non-standard region. *B*, wall thickness plotted *versus* time in a patient at 1 week and 3 months after a first-time myocardial infarction, showing wall thinning in the infarct zone owing to remodelling, together with functional augmentation in the remote zone (Sutton & Sharpe, 2000).

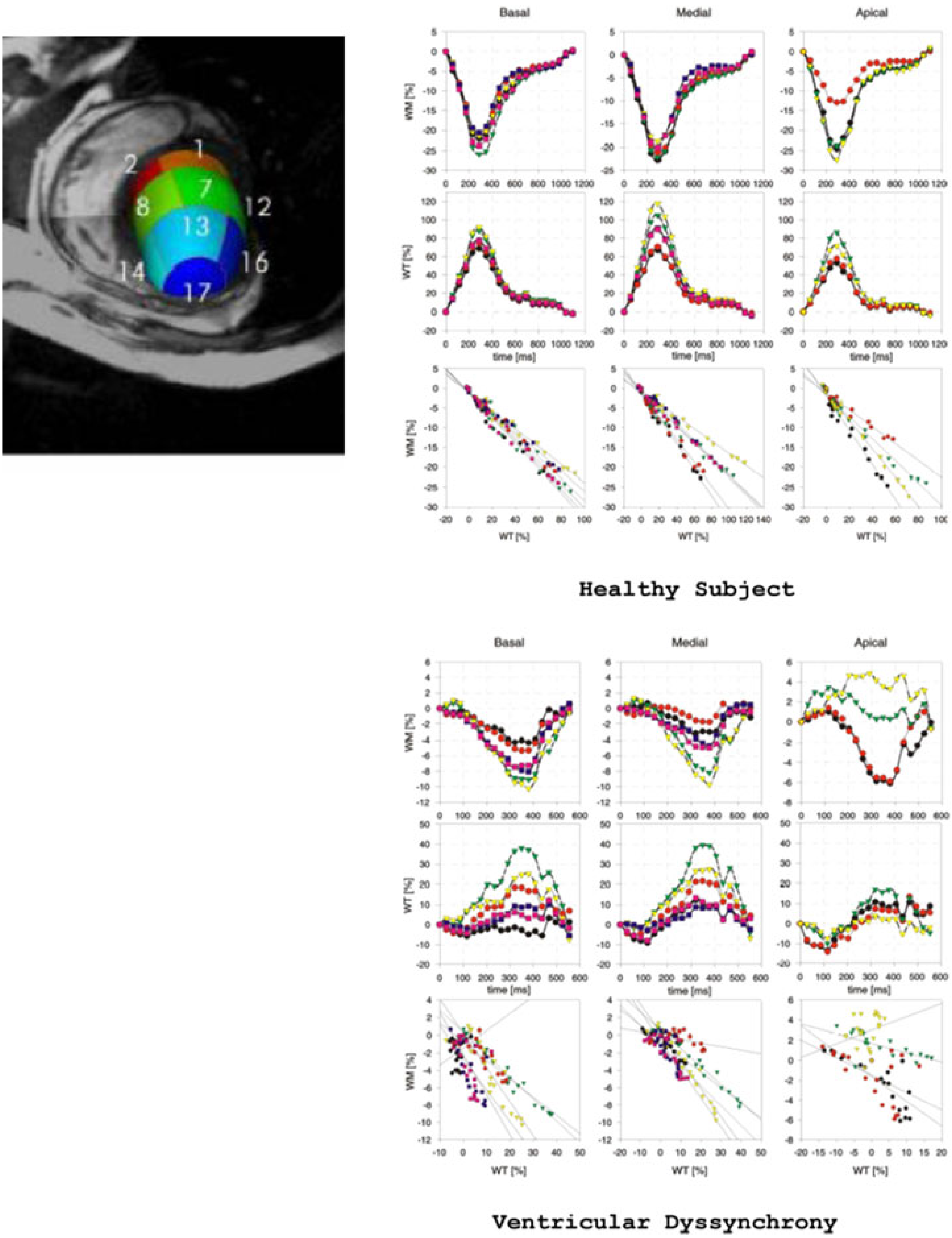

Figure 4. Model-based indices of asynchronous contraction
The left-hand panel shows a diastolic frame of a cardiac MRI sequence where the left ventricle has been segmented through model-based image analysis. Overlaid on the model are the various sectors of a bullseye representation. The right-hand panels show contractility patterns of a healthy subject and a cardiac resynchronization therapy candidate. The upper row plots the wall motion (WM) against time, while the middle row provides the curves of wall thickening (WT) against time. The lower row plots WM *versus* WT, showing clearly distinct patterns in both subject groups, which might aid in patient selection for therapy (Ordas *et al.* 2006).

Parametric distribution models

By customizing mathematical models of the anatomy and function of the heart to individual cases, it is possible to construct parameter variation models describing the distribution of regional cardiac shape and function across patient subgroups. Cootes *et al.* (1994) pioneered the application of Point Distribution Models (PDM) in computer vision problems. Homologous landmarks (i.e. the points which are aligned to match corresponding features in the shape) were used to characterize shape and shape variations with the aid of a principal component analysis. Since mathematical models, represented by the model parameters, are a complete and efficient characterization of cardiac shape and motion, a principal component analysis of the cardiac shape and motion models can be formed.

For example, in R dimensions, a set of M parameters can be defined in homologous locations around the heart. Bezier control points can be used as the global finite element parameters, since the scales of these parameters are all the same (unlike, for example, cubic Hermite parameters). Scaling between hearts can be corrected by scaling the parameters with respect to the apex–base length of the model. The pose (rotation and translation) is registered with each model due to the definition of the cardiac co-ordinate system. A database of N shapes is constructed, each represented by a vector of global nodal parameters $\mathbf{X}_n$, $n = 1, \ldots, N$, of length M. These parameters can then be used to construct a Parameter Distribution Model in the same manner as the traditional Point Distribution Models (Remme *et al.* 2005). The mean shape, $\mathbf{X}_m$, is:

$$\mathbf{X}_m = \frac{1}{N}\sum_{n=1}^{N}\mathbf{X}_n \qquad (1)$$

The modes of variation about the mean can be found by forming an $M \times N$ matrix of deviations from the mean:

$$B = \left[\mathbf{X}_1 \,\big|\!-\!\big|\, \mathbf{X}_m \quad \mathbf{X}_2 \,\big|\!-\!\big|\, \mathbf{X}_m \cdots \mathbf{X}_n \,\big|\!-\!\big|\, \mathbf{X}_m\right] \qquad (2)$$

from which the covariance matrix, C, can be calculated: $C = N^{-1}BB^T$. The eigenvalues and vectors of the covariance matrix can be found by singular value decomposition: $C = QDQ^T$, where D is a diagonal matrix of eigenvalues and Q is an orthogonal matrix of eigenvectors. If the data are distributed normally, the eigenvalues are the variances of the multidimensional normal distribution, and the eigenvectors determine the modes associated with the corresponding variance. The eigenvectors of the covariance matrix corresponding to the largest eigenvalues describe the most significant modes of variation in the dataset. Typically, most of the variation can be explained by a small number of modes, $K < \min(M, N)$, due to noise and redundancy in the dataset. In the following, we ignore the small modes of variation, so that the covariance matrix is then modeled as $\hat{C} = Q_K \Lambda Q_K^T$, where Λ is a $K \times K$ diagonal matrix and Q_K is an $M \times K$ matrix of significant shape modes. Any shape represented by a parameter vector $\mathbf{Y}$ can then be approximated in the PDM by a weighted sum of the modes, $\hat{\mathbf{Y}} = \mathbf{X}_m + Q_K\mathbf{b}$, where $\mathbf{b}$ is a $(K \times 1)$ vector of weights, one for each mode. The modes are orthogonal, so $Q_K^T Q_K = I(K \times K)$ and $\mathbf{b} = Q_K^T(\mathbf{Y} - \mathbf{X}_m)$ is the least squares solution to the problem of finding the closest model in the distribution to the given model $\mathbf{Y}$. We can generate new shapes by varying the weights $\mathbf{b}$ within suitable limits, which can be derived by examining the distributions of the values required to generate the database. If normal distributions are assumed, the logarithmic probability of obtaining a shape $\mathbf{Y}$ from the distribution is proportional to the Mahalanobis distance

$$\begin{aligned} D_m^2 &= (\hat{\mathbf{Y}} - \mathbf{X}_m)^T \hat{C}^{-1} (\hat{\mathbf{Y}} - \mathbf{X}_m) \\ &= (Q_K\mathbf{b})^T Q_K \Lambda^{-1} Q_K^T (Q_K\mathbf{b}) = \mathbf{b}^T \Lambda^{-1}\mathbf{b} = \sum_{i=1}^{K}\frac{b_i^2}{\lambda_i} \qquad (3) \end{aligned}$$

where λ_i is the ith eigenvalue of C.

The main modes of shape and motion variation can be plotted by looking at the range $-2\sqrt{\lambda_i} \le b_i \le 2\sqrt{\lambda_i}$, i.e. two standard deviations about the mean, which should encompass 95% of the shape variation of that mode. The effectiveness of these methods to detect regional wall motion abnormalities will be enhanced with the growth of such databases of normal and abnormal cases.

One of the largest-scale statistical cardiac atlases built so far has been based on multidetector computed tomography (MDCT) in a population of over 100 subjects and 15 phases of the cardiac cycle (Ordas *et al.* 2007; Fig. 5).

Clinical functional modes

Although the principal component analysis provides orthogonal (i.e. mathematically uncoupled) modes of deformation, the modes may not correspond to any intuitive or simple deformation. Figure 6*A* shows the mean values ± 2 S.D. in the three modes showing the greatest shape variation in a small database of normal volunteers (Augenstein & Young, 2001). In this plot, both end-diastolic and end-systolic models are included in each $\mathbf{X}_i$ parameter vector. The resulting models thus determine both the shape and the motion between end-diastole and end-systole. Clinically, these modes can be difficult to interpret, because they combine longitudinal with radial and torsional components. In an attempt to provide more clinically understandable modes of deformation, Remme *et al.* (2004) described a set of 'clinical' modes of variation and used these to characterize the differences between healthy volunteers and patients with type II diabetes. The deformation modes were chosen to decompose the deformation into clinically meaningful components, including apex–base shortening, wall thickening and ventricular torsion (Park *et al.* 1994; Remme *et al.* 2004). Figure 6*B* shows the definition of the modes of ventricular deformation, and Fig. 6*C* shows the distribution of the amount of each mode in a group of 15 healthy volunteers relative to a group of 30 patients with type II diabetes who had clinical evidence of diastolic dysfunction but normal systolic chamber function (Remme *et al.* 2004).

Related work is that of Suinesiaputra *et al.* (2009) where, instead of an *a priori* selection of modes based on clinical relevance to a specific disease, Independent Component Analysis (ICA) was used as a statistical method for selecting a shape base. Independent Component Analysis was shown to provide local support shape functions which, in addition, are independent from each other. This independence allows efficient estimation of the probability density function (PDF) of each parameter based on a training population of normal subjects. By propagating the PDFs of the ICA components to the spatial domain, one is able to make a local estimate of the probabilities of abnormal myocardial contraction (Fig. 7). The authors showed that areas of high probability of abnormal myocardial contraction corresponded to hyperenhancement in gadolinium-enhanced MR (Suinesiaputra *et al.* 2004).

Adapting population atlases to patient images

One of the beauties of statistical shape models is that they coherently unify the concepts of population atlases and model-based image analysis. In addition to providing a framework for parameterizing the mean anatomy and its variability, they also provide iterative schemes for progressively adapting the average atlas to a subject's image by an alternating process of model feature finding in the images and model parameter regression from image evidence. A recent algorithmic overview of this methodology is provided in the book of Davies *et al.* (2008), while their applications in medical and cardiac imaging are overviewed by Lelieveldt *et al.* (2005) and Frangi *et al.* (2005).

A number of techniques are available to perform model-to-image adaptation within the statistical shape modelling context applied to cardiac image analysis. Here we focus primarily on fully 3-D and 3-D+*t* techniques. Lotjonen *et al.* (2004) proposed a 3-D statistical shape model of the ventricles and atria and used it for segmentation purposes. van Assen *et al.* (2008) presented a method which uses fuzzy-logic techniques to recognize boundary images in MRI and CT images. van Assen *et al.* (2006) proposed a technique, which allows for fitting the models to arbitrarily oriented image acquisition planes. This is particularly important in MRI and 3-D ultrasound imaging, where non-planar image acquisition planes are customary in certain protocols. Lekadir *et al.* (2007) propose a technique for handling outliers during the feature-finding step in

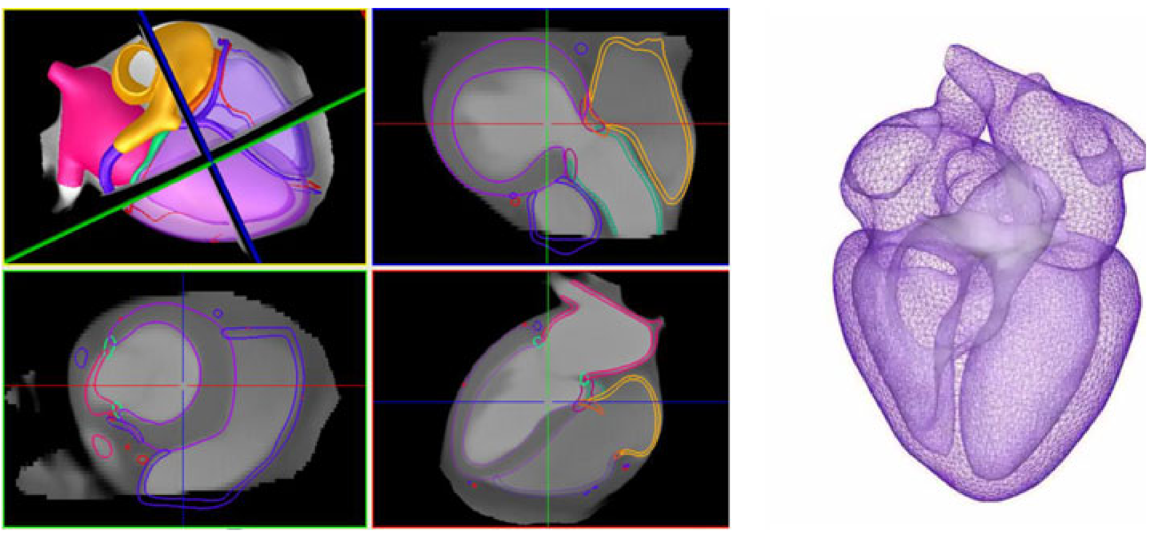

Figure 5. Whole-heart statistical atlas based on a population of about 100 subjects scanned with multidetector computed tomography, each over 15 time points in the cardiac cycle

The right panel shows the overlay of the average model on the CT-based atlas. The left panel shows a 3D surface rendered version of the average whole-heart model (Ordas *et al*. 2007). Each model node is labelled based on the anatomical substructure it belongs to. The statistical model has a representation of the average cardiac anatomy as well as a parameterization of the principal components of anatomical variations in the population.

order to make the fitting robust to missing boundary evidence. Other variations on statistical shape models proposed in the literature are the work developed by Lorenz & von Berg (2006), von Berg & Lorenz (2007) and Ecabert *et al.* (2008).

One approach, outlined by Remme *et al.* (2005), shows how statistical parameter distribution models derived from tagged MRI data can be used to guide the reconstruction of motion from other imaging protocols, such as cine imaging. Myocardial strains estimated from tracking features in untagged images matched well with a mean difference of 0.1 ± 3.2 and $0.3 \pm 3.0\%$ in circumferential and longitudinal strains, respectively. The calculated apex–base twist angle at end-systole had a mean difference of 1.0 ± 2.3 deg. This shows that sparse feature tracking in conjunction with a PDM provides accurate reconstruction of LV deformation in normal subjects.

Tobon-Gomez *et al.* (2008) have recently proposed a strategy to train intensity features for statistical models based on modelling and simulating the physics of image acquisition. This significantly reduces the burden associated with manual contouring of training images and enables reuse of point distribution models built based on other imaging modalities. In this particular paper, point distribution models were obtained from MDCT but applied to the segmentation of gated SPECT images. Ordas *et al.* (2007) developed an anatomical population model which, owing to the labelling of each of its nodes into

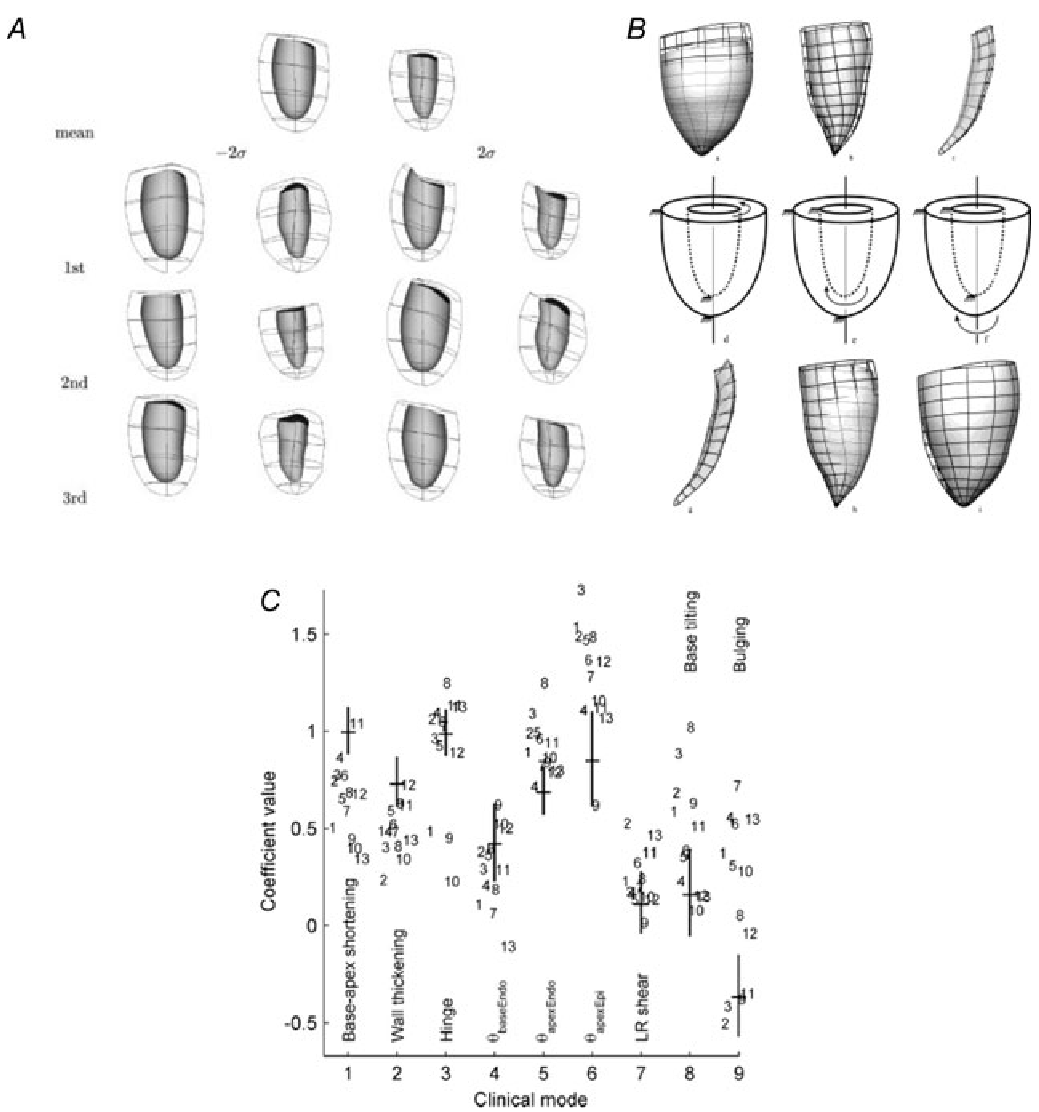

Figure 6. Statistical analysis of heart morphology and kinematics
A, principal components of shape and motion showing mean (top) and first three modes ± 2 S.D. (Augenstein & Young, 2001). *B*, definition of nine clinical modes of heart deformation. *C*, distribution of amount of motion in each clinical mode in patients with type II diabetes (numbers) compared with normal volunteers (means ± S.D. shown as cross-hairs). Panel B reproduced from Remme *et al.* (2004; ©, 2004 IEEE).

anatomical subparts, lends itself to be restricted to the cardiac structures which fall within the region of interest of the target modality. Figure 8 shows how such a model can be applied to various imaging modalities. A number of tools are being developed to make these technologies accessible to the scientific community. One such tool is the Graphical Interface for Medical Image Analysis and Simulation (GIMIAS), available at www.gimias.org.

Automated atlas construction from large databases

Computational cardiac atlases comprising statistical shape models are an exciting avenue for the coherent performance of anatomical phenotyping of cardiac diseases through model-based image analysis and advanced spatio-temporal morphometrics (Cootes & Taylor, 2007). However, an inherent weakness is that potentially, their performance in all these applications depends heavily on the careful selection of the training population and the laborious atlas-building procedure. This usually involves concomitant manual annotation of the images by experts, which is subjective and labour intensive.

Over the last decade, a number of authors have worked on developing techniques for automatic atlas building. A number of methods have been devised and applied to the cardiac (Frangi *et al.* 2002; Lorenz & von Berg, 2006) and other domains (Brett & Taylor, 1999; Davies *et al.* 2002; Rueckert *et al.* 2003; Cootes *et al.* 2004) that enable automatic landmarking of databases of either surface or image description of objects. Furthermore, some recent work has combined such methods with grid computing techniques in databases of over a thousand volume samples, therefore demonstrating the feasibility of large-scale atlas construction (Ordas *et al.* 2007). Among the most important recent developments in statistical shape models are those that aim at building the statistical models directly on the volumetric image representation using non-rigid registration techniques. One of the challenges ahead is to develop both the methods and the infrastructure to build statistical models directly from clinical image repositories and for a selective subpopulation of subjects (e.g. normal subjects or those affected with a specific disease).

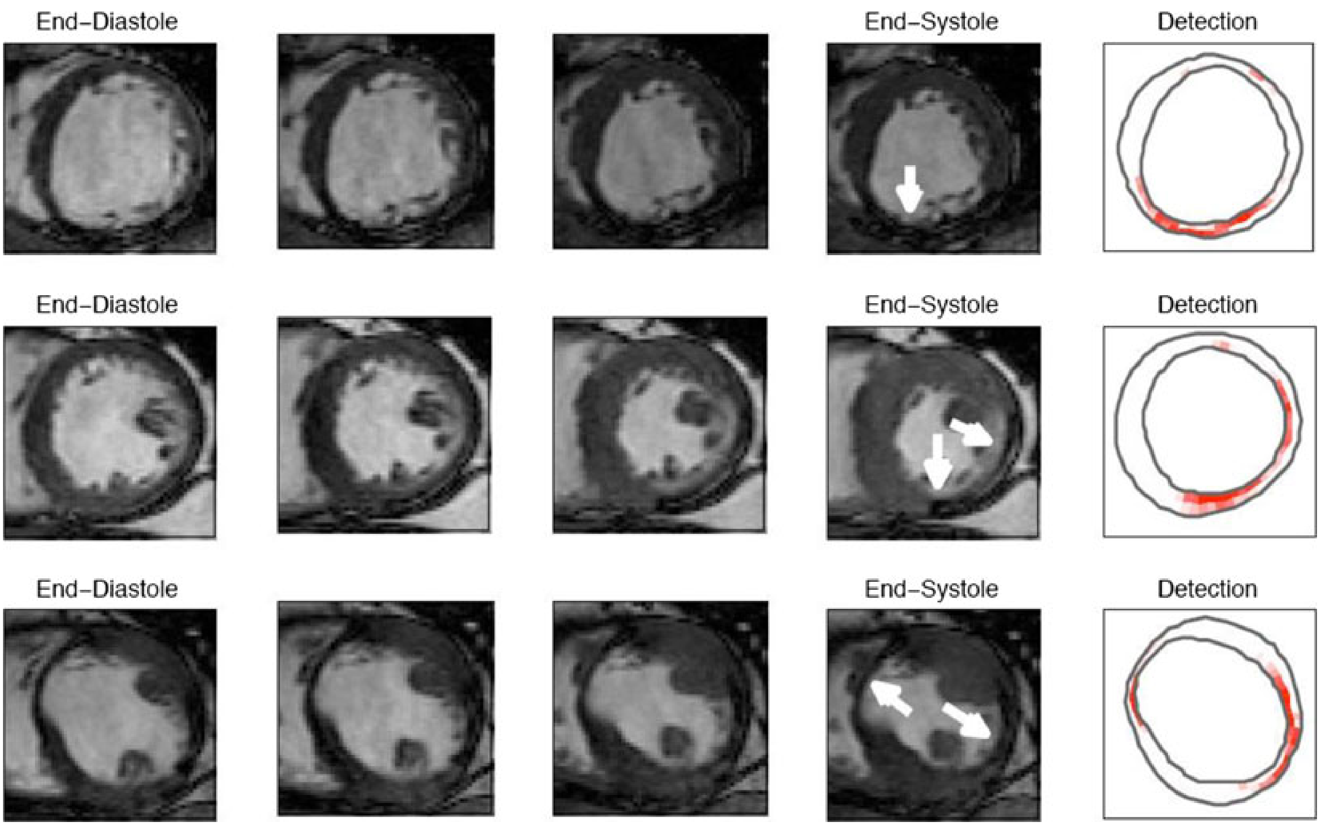

Figure 7. Three automated detection results (right panels) compared with the associated myocardial motion taken from MR image sequences (four frames from end-diastole to end-systole)
Grey shading in the rightmost column shows high probability of having an abnormal motion. White arrows in the end-systole images show corresponding regional areas of wall motion abnormality with the automated detection. Adapted from Suinesiaputra *et al*. (2009; ©, 2009 IEEE).

Multimodal fusion

Mathematical modelling of the heart enables registration and fusion of data from different imaging modalities and protocols. In one study, model-based methods for mapping regional strain and wall motion in relation to tissue characterization maps were developed and applied to a mouse model of reperfused myocardial infarction (Young *et al.* 2006). Magnetic resonance imaging tissue tagging was analysed in each short- and long-axis image using a semi-automated active contour process, and the 3-D motion reconstructed with the aid of the finite element model (Young *et al.* 1995), resulting in a dynamic model of LV deformation. The Lagrangian Green strain components between end-diastole and each subsequent time were calculated at specific finite element material points using standard methods of continuum mechanics (Fung, 1965). Previous validation experiments using a deformable silicone gel phantom have shown that this procedure produces accurate, unbiased estimates of displacement and shortening (Young *et al.* 1995).

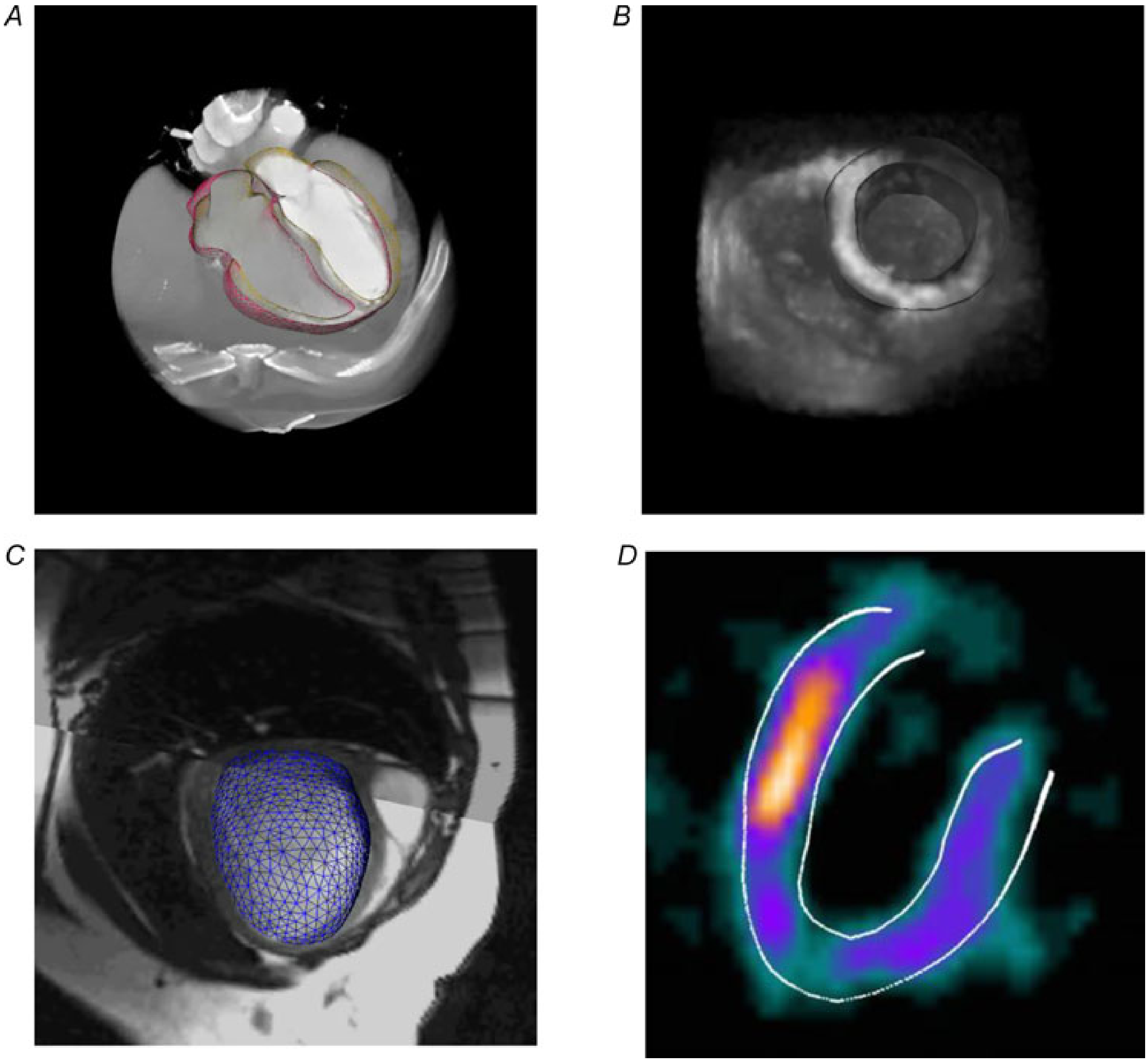

Figure 8. Examples of mode-to-image fitting to various cardiac imaging modalities involving different fields of view

A shows model adaptation to MDCT; *B* shows adaptation to three-dimensional US; *C* demonstrates model fitting to left ventricular endocardial borders in MRI; and *D* shows model fitting to gated SPECT. One could conceive using the reconstructed models to define a common reference system for mapping the various imaging modalities so that interrelationships between structure and function can be established. Note that although the underlying model stays equivalent, the image appearance can be quite different. Note also how gaps and holes in image information (e.g. those coming from perfusion defects in SPECT) can be effectively handled by using statistical information on cardiac anatomy.

Infarcted regions, as defined by regions of late gadolinium enhancement, were outlined on each image in the short-axis stack (Fig. 9*e* and *f*). The image co-ordinates of the contours were then transformed into 3-D magnet co-ordinates using the 3-D location of the image planes. The magnet co-ordinates were then transformed into a bullseye plot of the left ventricle (Fig. 9*g*). A convex perimeter was manually drawn on the bullseye map so as to enclose the hyperenhancement contours (Fig. 9*g*). The bullseye co-ordinates of the perimeter were then converted to 3-D cardiac co-ordinates and projected in the transmural direction onto the mid-wall surface of the LV finite element model. This allowed the calculation of the 3-D infarct geometry in finite element material co-ordinates. The 3-D infarct geometry was fixed onto the dynamic finite element model at end-diastole, and allowed to deform with the beating model during systole and diastole (Fig. 9*h*).

Material points within the finite element model were assigned to regions relative to the 3-D infarct geometry as follows. Points within the 3-D infarct geometry were denoted '*infarct*', points within 1.0 mm of the 3-D infarct geometry (but outside it) were denoted '*adjacent*', and all other points were denoted '*remote*'. This procedure also allowed calculation of the percentage of myocardium in the infarct, adjacent and remote zones, respectively. Since the models were defined in a co-ordinate system aligned with each heart, a material point could be mapped onto the corresponding material point at each time point during remodelling.

Fusion of *in vivo* MRI tagging and *ex vivo* diffusion tensor magnetic resonance imaging (DTMRI) relates functional stain information with structural fibre orientation. DTMRI images the diffusion tensor and the direction of maximal water diffusion (the primary eigenvector) in each voxel of the DTMRI image directly relates to the myocardial fibre orientation. Free-form deformation methods (Fig. 10) have been developed which enable feature-based registration between image modalities (Lam *et al.* 2007).

Biomechanical analysis

Biophysically based computational models of cardiac structure and function can be customized to individual patient images by optimizing the biophysical parameters underlying normal and pathological function. The LV remodels its structure and function to adapt to pathophysiological changes in geometry and loading conditions, and this process can be understood in terms of adaptation of underlying biophysical parameters. Computational models have been developed of heart geometry (Nielsen *et al.* 1991*a*; LeGrice *et al.* 2001), microstructure (LeGrice *et al.* 1995, 1997; Hooks *et al.*

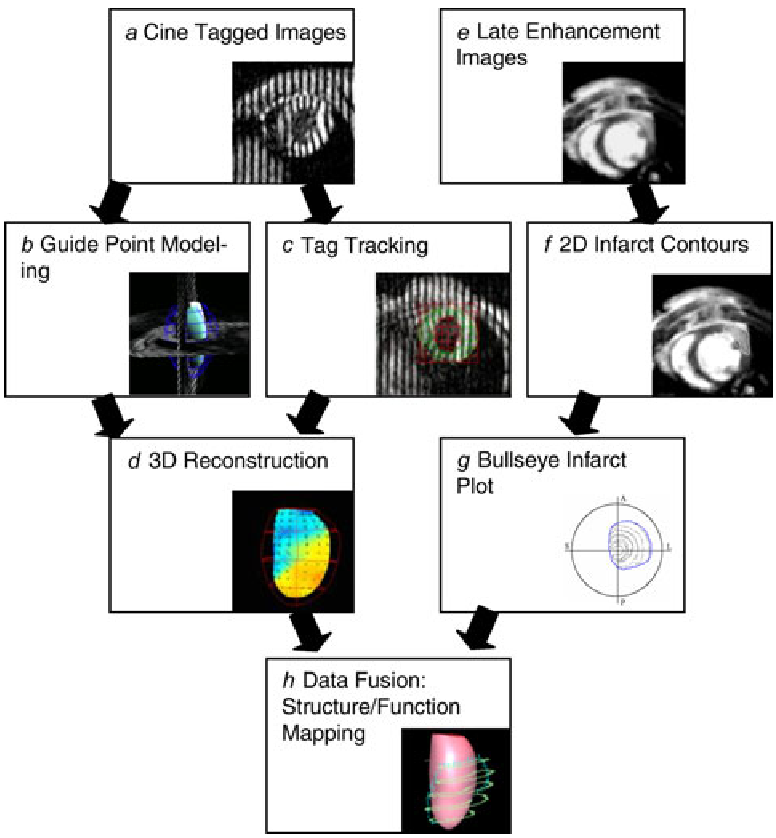

Figure 9. Flow chart of the modelling and data fusion process
Reproduced with permission from Young *et al.* (2006).

2002), material properties (Hunter & Smaill, 1988; Nielsen *et al.* 1991*b*; Dokos *et al.* 2002; Schmid *et al.* 2008), stress (Hunter *et al.* 1996, 1998; Costa *et al.* 1996*a,b*; Nash & Hunter, 2001), perfusion (Smith *et al.* 2000, 2002), cellular electromechanics (Nickerson *et al.* 2001) and activation (Hunter *et al.* 1996; Bradley *et al.* 2000; Mulquiney *et al.* 2001; Hooks *et al.* 2002). Cellular mechanisms, including membrane channel characteristics, excitation–contraction coupling and cross-bridge cycling dynamics, can be incorporated into a continuum description of the whole organ. Image data can be used to optimize the parameters of such models, for example determining the material stiffness of the tissue from knowledge of tissue deformation and boundary conditions.

Augenstein *et al.* (2006) developed a method for *in vitro* identification of material parameters from MRI tissue tagging and DTMRI. These methods were extended to the *in vivo* situation by Wang *et al.* (2008). Given information on the geometry and deformation (from MRI tissue tagging), and muscle microstructure (DTMRI) pressure boundary conditions from time-matched recordings, parameters of an integrated finite element model simulation of LV mechanics can be optimized to the data. The observed LV deformation obtained from tagged MRI data provides the necessary kinematic data required to validate the model and estimate the constitutive properties of the passive myocardium (Fig. 11). These integrated physiological models will allow more insight into the mechanics of the LV on an individualized basis, thereby improving our understanding of the underlying structural basis of mechanical dysfunction in pathological conditions.

Electrophysiological analysis

As for the individualization of biomechanical models, subject-specific models of cardiac electrophysiology and cardiac electromechanics can be constructed by combining anatomical models derived from structural imaging, and tissue distributions and their properties as obtained from functional imaging. In some cases, the results from these simulations can be compared or informed with measurements obtained through dynamic imaging or body surface or intracavitary potential mapping. Ultimately, the goal of such combination of imaging and electrophysiological/electromechanical models is to extend the diagnostic capabilities of the present imaging systems with predictive capacity for variables which usually require invasive electrophysiological mapping procedures. In addition, this predictive capacity will contribute to the interventional planning and to the customization and optimization of interventional procedures (Rhode *et al.* 2005) such as radio frequency ablation (Sermesant *et al.* 2003, 2005; Reumann *et al.* 2008; Plank *et al.* 2008) or cardiac resynchronization therapy (CRT; Reumann *et al.* 2007; Sermesant *et al.* 2008; Romero *et al.* 2008).

The present available electrophysiological models, ranging from single cell (Noble & Rudy, 2001; ten Tusscher *et al.* 2004; Fenton *et al.* 2005; ten Tusscher & Panfilov 2006) to tissue level (Henriquez & Papazoglou 1996; Pollard & Barr, 1991; Pollard *et al.* 1993) and organ level (Noble, 2004, 2007; Trayanova, 2006; Vigmond *et al.* 2008*a*), have proved sufficiently accurate to model complex processes, including ion kinetics in healthy and pathological conditions. In many cases, cardiac modelling can be used to investigate phenomena such as drug effects on the electromechanical response and arrhythmogenesis (Henriquez & Papazoglou, 1996; Packer, 2004; Rodriguez *et al.* 2005), which are difficult to study *in vivo*.

When the main goal of such modelling approaches is their application in diagnostic or treatment planning settings, it is essential to be able to personalize them with patient-specific data, for instance, by data assimilation techniques (Sermesant *et al.* 2006). This has shown, for instance, in the influence of a number of parameters in the activation sequence of the paced heart, such as the geometry of the heart (e.g. induced by specific pathologies such as dilated cardiomyopathies or cardiac hypertrophy) or specific assumptions in the Purkinje System model (Vigmond *et al.* 2008*a,b*). Recently, these effects have been investigated by analysing and comparing the activation pattern in biventricularly paced hearts, both in normal hearts and in hypertrophic and dilated hearts.

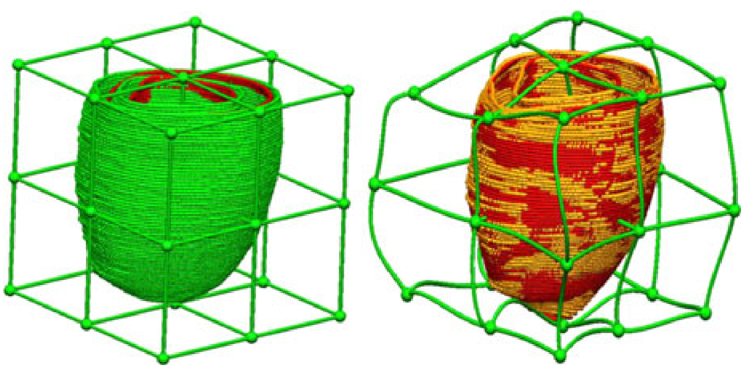

Figure 10. Free form deformation registration between DTMRI and tagged MRI
Left panels shows that host mesh fitting involved minimizing the distance between landmark points (DTI segmented contours, shaded pale grey) and target points (the projections of DTMRI contours onto the LV model, shaded dark grey) using a simple 8−element tri-Cubic Hermite host mesh. Right panel shows the deformed host mesh with transformed DTMRI surface data.

The main conclusion of this work is that pathology-induced anatomical distortions can provoke important changes in the activation sequences and thus they need to be accounted for when planning the positioning of pacing leads (Fig. 12). Therefore, therapy optimization requires the use of advanced image analysis and simulation tools either on a per subject basis or, at least, performing population studies *in silico*. Such studies can lead to the identification of interventional guidelines or treatment criteria that minimize the effect of subject-specific variations, thus optimizing treatment outcome at a population level.

Conclusions

The creation and application of statistical atlases is a mature technology with some very promising results in the cardiac domain. Cardiac atlases provide a consistent framework for phenotyping disease in populations and individuals by parameterizing morphodynamic features, both in terms of average patterns and their population variability. A number of methods exist for automated atlas building and for their instantiation in multimodal imaging. The trend is towards unified model-to-image instantiation mechanisms that work across imaging modalities while sharing a common shape model to

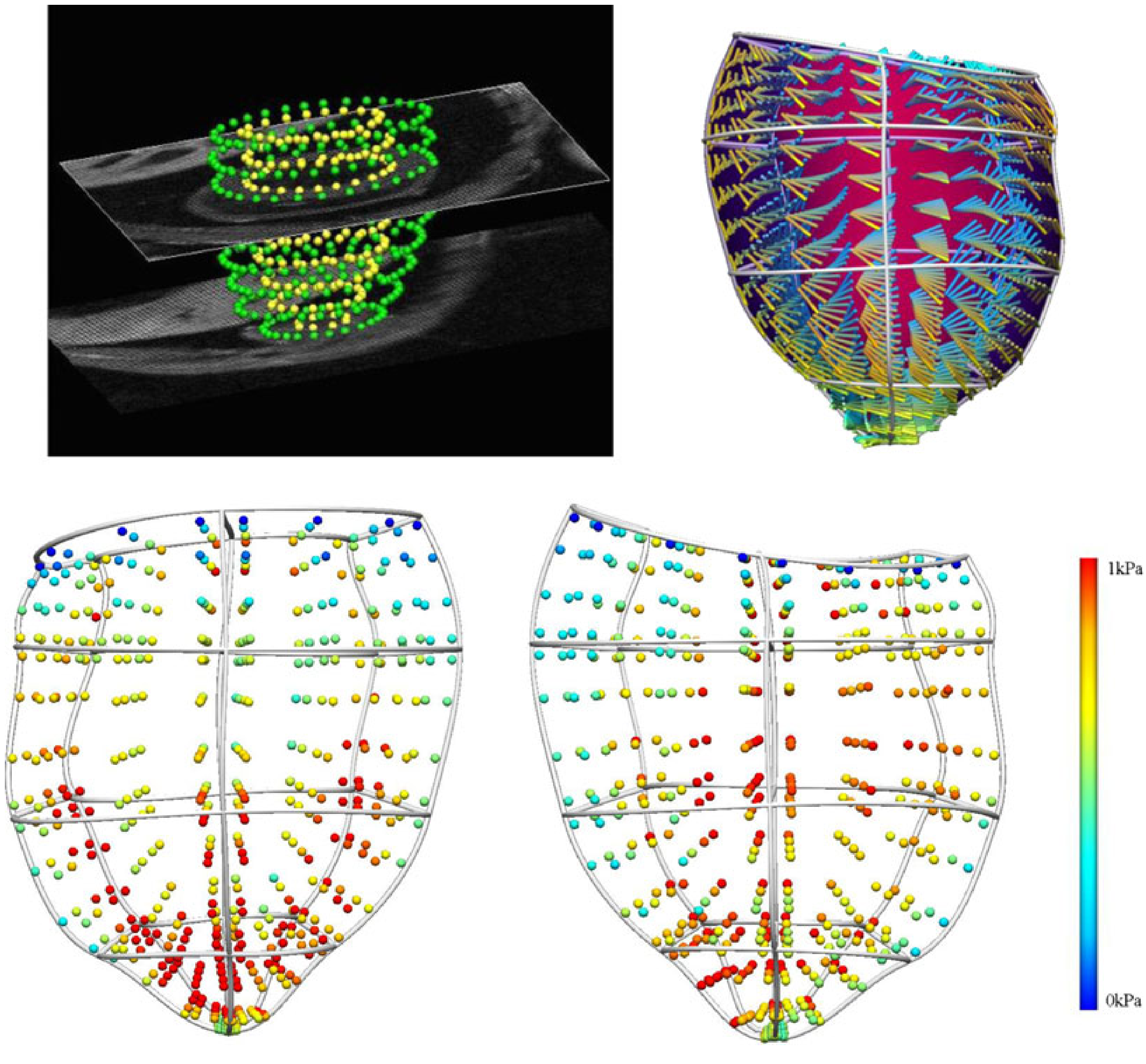

Figure 11. Data fusion and stress estimation
A, Zinc Digitizer screenshot showing segmented contours from short-axis images. *B*, posterior view of the LV (r.m.s. error = 0.3 mm) with fitted fibre vectors. Also shown are anterior (*C*) and posterior views (*D*) of the stress distribution at each Gauss point of the predicted end-diastolic model.

act as a common co-ordinate system. Among the applications of such models are a number of advanced image analysis tasks, as well as their integration into a computational physiology framework, yielding biomechanical or electrophysiological information.

Future work will include further automation and scalability of model-building procedures so that they can be used in large-scale image databases of the order of tens of thousands of images. Creation and curation of large-scale annotated reference databases will require emerging standards, such as FieldML (http://www.physiome.org.nz/xml_languages/fieldml). Incorporation into the statistical framework of physical and physiological constraints will facilitate or regularize subsequent exploitation in simulation applications. Incorporation of critical cardiac structures, such as the Purkinje system, fibre orientation and the coronary artery tree, will facilitate further biophysical modelling. Computational physiology models provide an exciting avenue for the integration and fusion of multimodal imaging and signals through physics- and physiology-based domain knowledge, which usually is preceded by more conventional image and signal registration steps to bring all this information into a coherent spatio-temporal co-ordinate system. We anticipate that an increased cross-fertilization between the imaging, modelling and simulation communities, in close dialogue with concrete diagnostic and interventional problems, will lead to focused and translational use of all these technologies and thus to a more effective exploitation of the currently available clinical data. Finally, the possibility of defining population subgroups, both in the atlas building and in the statistical modelling stages, may enable automatic identification of clusters of cardiac morphological patterns (e.g. resulting from changes in the topological structure of the parts) so that they can be modelled with non-linear statistical methods.

References

Augenstein KF, Cowan BR, LeGrice IJ & Young AA (2006). Estimation of cardiac hyperelastic material properties from MRI tissue tagging and diffusion tensor imaging. In *Medical Image Computing and Computer-Aided Intervention – MICCAI 2006*, LNCS 4190, ed. Larsen R, Nielsen M & Sporring J, vol. I, pp. 628–635. Springer, Berlin.

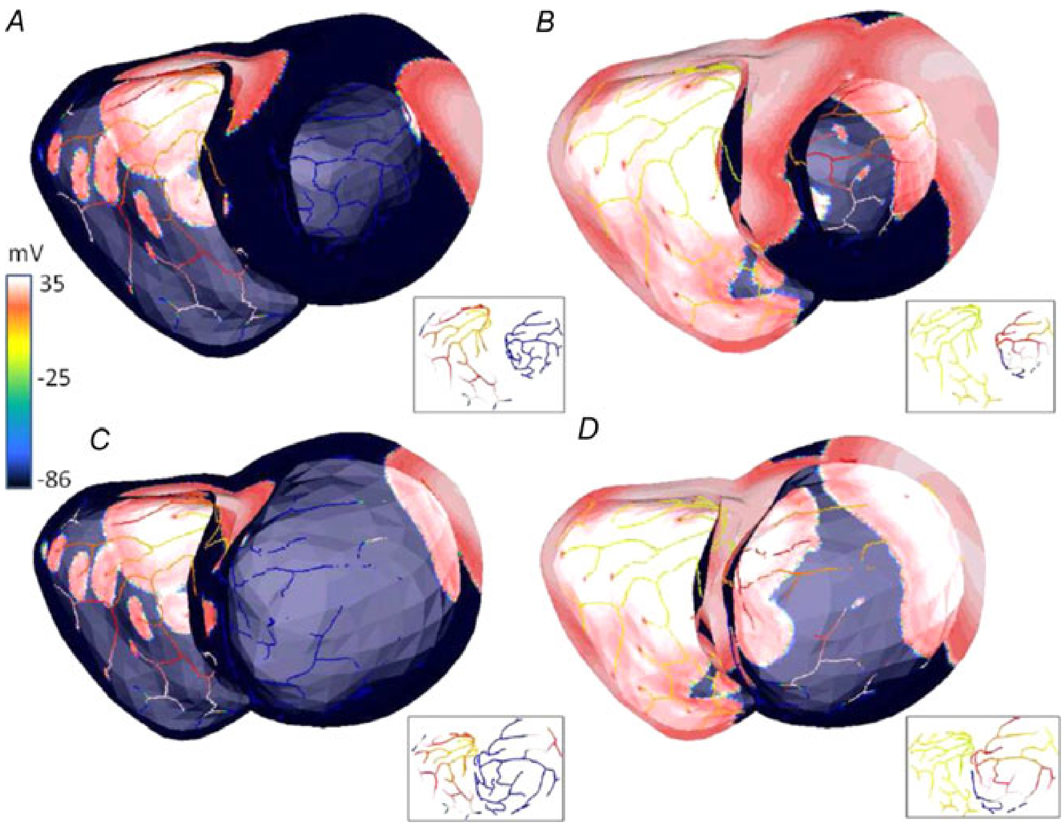

Figure 12. Activation of the hypertrophic and dilated models from a biventricular pacemaker with simultaneous activation of the pacemaker leads

A and *B* correspond to the hypertrophic and *C* and *D* to the dilated model. The activations are displayed 40 (*A* and *C*) and 60 ms (*B* and *D*) after the CRT lead stimulus. Colours represent the transmembrane potential at each point of the mesh. The inset for each panel depicts the progress of the Purkinje system activation at the same time points. All the views are basal. Image courtesy of D. Romero and R. Sebastian, based on the CARP Software Package (Vigmond *et al.* 2008).

Augenstein KF & Young AA (2001). Finite element modeling for three-dimensional motion reconstruction and analysis. In *Measurement of Cardiac Deformations from MRI: Physical and Mathematical Models*, ed. Amini AA & Prince JL, pp. 37–58. Kluwer Academic Publishers, Dordrecht, The Netherlands.

Beg MF, Helm PA, McVeigh E, Miller MI & Winslow RL (2004). Computational cardiac anatomy using MRI. *Magn Reson Med* **52**, 1167–1174.

Bottini PB, Carr AA, Prisant LM, Flickinger FW, Allison JD & Gottdiener JS (1995). Magnetic resonance imaging compared to echocardiography to assess left ventricular mass in the hypertensive patient. *Am J Hypertens* **8**, 221–228.

Bradley CP, Pullan AJ & Hunter PJ (2000). Effects of material properties and geometry on electrocardiographic forward simulations. *Ann Biomed Eng* **28**, 721–741.

Brett AD & Taylor CJ (1999). A framework for automated landmark generation for automated 3D statistical model construction. In *16th Conference on Information Processing in Medical Imaging*, Visegrád, Hungary, pp. 376–381. Springer, Berlin.

Cootes TF, Hill A, Taylor CJ & Haslam J (1994). The use of active shape models for locating structures in medical images. *Image Vision Comput* **12**, 355–366.

Cootes TF, Marsland S, Twining CJ, Smith K & Taylor CJ (2004). Groupwise diffeomorphic non-rigid registration for automatic model building. In *8th European Conference on Computer Vision*, vol. 4, pp. 316–327. Springer, Berlin.

Cootes TF & Taylor CJ (2007). Anatomical statistical models and their role in feature extraction. *Br J Radiol* **77**, S133–S139.

Costa KD, Hunter PJ, Rogers JM, Guccione JM, Waldman LK & McCulloch AD (1996*a*). A three-dimensional finite element method for large elastic deformations of ventricular myocardium: Part I – Cylindrical and spherical polar coordinates. *ASME J Biomech En* **118**, 452–463.

Costa KD, Hunter PJ, Wayne JS, Waldman LK, Guccione JM & McCulloch AD (1996*b*). A three-dimensional finite element method for large elastic deformations of ventricular myocardium: Part II – Prolate spherical coordinates. *ASME J Biomech Eng* **118**, 464–472.

Davies R, Twining CJ & Taylor CJ (2008). *Statistical Models of Shape: Optimisation and Evaluation*. Springer, Berlin.

Davies RH, Twining CJ, Cootes TF, Waterton JC & Taylor CJ (2002). A minimum description length approach to statistical shape modeling. *IEEE Trans Med Imaging* **21**, 525–537.

Dokos S, Smaill BH, Young AA & Le Grice IJ (2002). Shear properties of passive ventricular myocardium. *Am J Physiol Heart Circ Physiol* **283**, H2650–H2659.

Ecabert O, Peters J, Schramm H, Lorenz C, von Berg J, Walker MJ, Vembar M, Olszewski ME, Subramanyan K, Lavi G & Weese J (2008). Automatic model-based segmentation of the heart in CT images. *IEEE Trans Med Imaging* **27**, 1189–1201.

Fenster A & Downey DB (2000). Three-dimensional ultrasound imaging. *Annu Rev Biomed Eng* **2**, 457–475.

Fenton FH, Cherry EM, Karma A & Rappel W-J (2005). Modeling wave propagation in realistic heart geometries using the phase-field method. *Chaos* **15**, 13502.

Fonseca CG, Dissanayake AM, Doughty RN, Whalley GA, Gamble GD, Cowan BR, Occleshaw CJ & Young AA (2004). 3-D assessment of left ventricular systolic strain in patients with type 2 diabetes mellitus, diastolic dysfunction and normal ejection fraction. *Am J Cardiol* **94**, 1391–1395.

Frangi AF, Niessen WJ, Viergever MA & Lelieveldt BPF (2005). A survey of three-dimensional modeling techniques for quantitative functional analysis of cardiac images. In *Advanced Image Processing in MRI*, pp. 267–344, CRC Press, London.

Frangi AF, Rueckert D, Schnabel JA & Niessen W (2002). Automatic construction of multiple-object three-dimensional statistical shape models: application to cardiac modeling. *IEEE Trans Med Imaging* **21**, 1151–1165.

Fung YC (1965). *Foundations of Solid Mechanics*, pp. 97. Prentice Hall, Englewood Cliffs, NJ, USA.

Goldin JG, Ratib O & Aberle DR (2000). Contemporary cardiac imaging: an overview. *J Thorac Imaging* **15**, 218–229.

Henriquez C & Papazoglou A (1996). Using computer models to understand the roles of tissue structure and membrane dynamics in arrhythmogenesis. *Proc IEEE* **84**, 334–354.

Hoogendoorn C, Sukno FM, Ordas S & Frangi AF (2007). Bilinear models for spatio-temporal point distribution analysis: application to extrapolation of whole heart cardiac dynamics. In *Proceedings of Mathematical Methods in Biomedical Image Analysis*, pp. 1–8. IEEE Computer Society Press, Rio de Janeiro, Brazil.

Hoogendoorn C, Sukno FM, Ordas S & Frangi AF (2009). Bilinear models for spatiotemporal point distribution analysis: application to extrapolation of left ventricular, biventricular and whole heart cardiac dynamics. *Int J Comp Vis*, in press.

Hooks DA, Tomlinson KA, Marsden SG, LeGrice IJ, Smaill BH, Pullan AJ & Hunter PJ (2002). Cardiac microstructure: implications for electrical propagation and defibrillation in the heart. *Circ Res* **91**, 331–338.

Hsu EW, Muzikant AL, Matulevicius SA, Penland RC & Henriquez CS (1998). Magnetic resonance myocardial fiber-orientation mapping with direct histological correlation. *Am J Physiol Heart Circ Physiol* **274**, H1627–H1634.

Hu H (1999). Multi-slice helical CT: scan and reconstruction. *Med Phys* **26**, 5–18.

Hunter PJ, McCulloch AD & ter Keurs HE (1998). Modelling the mechanical properties of cardiac muscle. *Prog Biophys Mol Biol* **69**, 289–331.

Hunter PJ, Nash MP & Sands GB (1996). Computational electro-mechanics of the heart. In *Computational Biology of the Heart*, ed. Panfilov A & Holden A, pp. 347–409. John Wiley Series on Nonlinear Science.

Hunter PJ & Smaill BH (1988). The analysis of cardiac function: a continuum approach. *Prog Biophys Mol Biol* **52**, 101–164.

Kilner PJ, Yang GZ, Wilkes AJ, Mohiaddin RH, Firmin DN & Yacoub MH (2000). Asymmetric redirection of flow through the heart. *Nature* **404**, 759–761.

Kim RJ, Wu E, Rafael A, Chen E-L, Parker MA, Simonetti O, Klocke FJ, Bonow RO & Judd RM (2000). The use of contrast-enhanced magnetic resonance imaging to identify reversible myocardial dysfunction. *N Engl J Med* **343**, 1445–1453.

Klingenbeck-Regn K, Flohr T, Ohnesorge B, Regn J & Schaller S (2002). Strategies for cardiac CT imaging. *Int J Cardiovasc Imaging* **18**, 143–151.

Klingenbeck-Regn K, Schaller S, Flohr T, Ohnesorge B, Kopp AF & Baum U (1999). Subsecond multi-slice computed tomography: basics and applications. *Eur J Radiol* **31**, 110–124.

Lam HL, Wang VY, Nash MP & Young AA (2007). Aligning tagged and diffusion tensor MRI for ventricular function analysis. *Proc Biomedical Engineering Society* pp. 538.

Lange A, Palka P, Burstow DJ & Godman MJ (2001). Three-dimensional echocardiography: historical development and current applications. *J Am Soc Echocardiogr* **14**, 403–412.

Lees W (2001). Ultrasound imaging in three and four dimensions. *Semin Ultrasound CT MR* **22**, 85–105.

LeGrice I, Hunter P, Young A & Smaill B (2001). The architecture of the heart: a data-based model. *Phil Trans Roy Soc* **359**, 1217–1232.

LeGrice IJ, Hunter PJ & Smaill BH (1997). Laminar structure of the heart: a mathematical model. *Am J Physiol Heart Circ Physiol* **272**, H2466–H2476.

LeGrice IJ, Smaill BH, Chai LZ, Edgar SG, Gavin JB & Hunter PJ (1995). Laminar structure of the heart: ventricular myocyte arrangement and connective tissue architecture in the dog. *Am J Physiol Heart Circ Physiol* **269**, H571–H582.

Lekadir K, Merrifield R & Yang GZ (2007). Outlier detection and handling for robust 3-D active shape models search. *IEEE Trans Med Imaging* **26**, 212–222.

Lelieveldt BPF, Frangi AF, Mitchell SC, van Assen HC, Ordas S, Reiber Johan HC & Sonka M (2005). 3D active shape and appearance models in medical image analysis. In *Mathematical Models of Computer Vision: The Hand-book*, ed. Paragios N, Chen Y & Faugeras O, pp. 471–484, Springer, Berlin.

Lorenz C & von Berg J (2006). A comprehensive shape model of the heart. *Med Image Anal* **10**, 657–670.

Lotjonen J, Kivisto S, Koikkalainen J, Smutek D & Lauerma K (2004). Statistical shape model of atria, ventricles and epicardium from short- and long-axis MR images. *Med Image Anal* **8**, 371–386.

Mulquiney PJ, Smith NP, Clark K & Hunter PJ (2001). Mathematical modelling of the ischaemic heart. *Nonlinear Anal* **47**, 235–244.

Myerson SG, Bellenger NG & Pennell DJ (2002). Assessment of left ventricular mass by cardiovascular magnetic resonance. *Hypertension* **39**, 750–755.

Nash MP & Hunter PJ (2001). Computational mechanics of the heart. *J Elasticity* **61**, 113–141.

Nickerson DP, Smith NP & Hunter PJ (2001). A model of cardiac cellular electromechanics. *Phil Trans Royal Soc London* **359**, 1159–1172.

Nielsen PM, Le Grice IJ, Smaill BH & Hunter PJ (1991*a*). Mathematical model of geometry and fibrous structure of the heart. *Am J Physiol Heart Circ Physiol* **260**, H1365–H1378.

Nielsen PMF, Hunter PJ & Smaill BH (1991*b*). Biaxial testing of membrane biomaterials: testing equipment and procedures. *ASME J Biomech Eng* **113**, 295–300.

Noble D (2004). Modeling the heart. *Physiology (Bethesda)* **19**, 191–197.

Noble D (2007). From the Hodgkin–Huxley axon to the virtual heart. *J Physiol* **580**, 15–22.

Noble D & Rudy Y (2001). Models of cardiac ventricular action potentials: iterative interaction between experiment and simulation. *Philos Trans Math Phys Eng Sci* **359**, 1127–1142.

Ordas S, Oubel E, Sebastian R & Frangi AF. (2007). Computational anatomy atlas of the heart. *International Symposium on Image and Signal Processing and Analysis (ISPA), Istanbul, Turkey*, pp. 338–342. IBBB, Computer Society Press, Istanbul, Turkey.

Ordas S, Tobon C, Moure C, Huguet M & Frangi AF (2006). Automatic assessment of left ventricular contraction synchronicity in cine MRI studies. *Proceedings ISMRM 14th Scientific Meeting*, Seattle, USA. John Wiley & Sons, Chichester.

Oshinski JN, Yang Z, Jones JR, Mata JF & French BA (2001). Imaging time after Gd-DTPA injection is critical in using delayed enhancement to determine infarct size accurately with magnetic resonance imaging. *Circulation* **104**, 2838–2842.

Packer D (2004). Evolution of mapping and anatomic imaging of cardiac arrhythmias. *PACE* **27**, 1026–1049.

Panting JR, Gatehouse PD, Yang GZ, Grothues F, Firmin DN, Collins P & Pennell DJ (2002). Abnormal subendocardial perfusion in cardiac syndrome X detected by cardiovascular magnetic resonance imaging. *N Engl J Med* **346**, 1948–1953.

Park J, Metaxas D & Young AA (1994). Deformable models with parameter functions: application to heart wall modeling. *Proc Computer Vision and Pattern Recognition, Seattle, USA*, pp. 437–442. IBBB, Computer Society Press, Seattle, USA.

Pattynama PMT, DeRoos A, Vanerwall EE & Vanvoorthuisen AE (1994). Evaluation of cardiac function with magnetic resonance imaging. *Am Heart J* **128**, 595–607.

Perperidis D, Mohiaddin RH & Rueckert D (2005). Spatio-temporal free-form registration of cardiac MR image sequences. *Med Image Anal* **9**, 441–456.

Plank G, Zhou L, Greenstein JL, Cortassa S, Winslow RL, O'Rourke B & Trayanova NA (2008). From mitochondrial ion channels to arrhythmias in the heart: computational techniques to bridge the spatio-temporal scales. *Phil Trans A Math Phys Eng Sci* **366**, 3381–3409.

Pollard AE & Barr R (1991) Computer simulations of activation in an anatomically based model of the human ventricular conduction system. *IEEE Trans Biomed Eng* **38**, 982–996.

Pollard AE, Burgess MJ & Spitzer KW (1993). Computer simulations of three-dimensional propagation in ventricular myocardium. Effects of intramural fiber rotation and inhomogeneous conductivity on epicardial activation. *Circ Res* **72**, 744–756.

Pruessmann KP, Weiger M, Scheidegger MB & Boesiger P (1999). SENSE: sensitivity encoding for fast MRI. *Magn Reson Med* **42**, 952–962.

Reeder SB, Du YP, Lima JA & Bluemke DA (2001). Advanced cardiac MR imaging of ischemic heart disease. *Radiographics* **21**, 1047–1074.

Rehwald WG, Fieno DS, Chen E-L, Kim RJ & Judd RM (2002). Myocardial magnetic resonance imaging contrast agent concentrations after reversible and irreversible ischemic injury. *Circulation* **105**, 224–229.

Reichek N (1991). Magnetic resonance imaging for assessment of myocardial function. *Magn Reson Quart* **7**, 255–274.

Remme EW, Augenstein KF, Young AA & Hunter PJ (2005). Parameter distribution models for estimation of population based left ventricular deformation using sparse fiducial markers. *IEEE Trans Med Imaging* **24**, 381–388.

Remme EW, Young AA, Augenstein KF & Hunter PJ (2004). Extraction and quantification of left ventricular deformation modes. *IEEE Trans Biomed Eng* **51**, 1923–1931.

Reumann M, Bohnert J, Seemann G, Osswald B & Dössel O (2008). Preventive ablation strategies in a biophysical model of atrial fibrillation based on realistic anatomical data. *IEEE Trans Biomed Eng* **55**, 399–406.

Reumann M, Farina D, Miri R, Lurz S, Osswald B & Dössel O (2007). Computer model for the optimization of AV and VV delay in cardiac resynchronization therapy. *Med Biol Eng Comput* **45**, 845–854.

Rhode KS, Sermesant M, Brogan D, Hegde S, Hipwell J, Lambiase P, Rosenthal E, Bucknall C, Qureshi SA, Gill JS, Razavi R & Hill DL (2005). A system for real-time XMR guided cardiovascular intervention. *IEEE Trans Med Imaging* **24**, 1428–1440.

Rodriguez B, Li L, Eason JC, Efimov IR & Trayanova NA (2005). Differences between left and right ventricular chamber geometry affect cardiac vulnerability to electric shocks. *Circ Res* **97**, 168–175.

Romero DA, Sebastian R, Plank G, Vigmond EJ & Frangi AF (2008). Modeling the influence of the VV delay for CRT on the electrical activation patterns in absence of conduction through the AV node. In *SPIE Medical Imaging: Visualization, Image-guided procedures, and Modeling*, ed. Miga MI & Cleary KR, **vol. 6918**, p. G9182. SPIE, San Diego, USA.

Rueckert D & Burger P (1997). Shape-based segmentation and tracking of the heart in 4D cardiac MR images. In *Proc. of Medical Image Understanding and Analysis 1997*, Oxford University, UK, pp. 193–196.

Rueckert D, Frangi AF & Schnabel JA (2003). Automatic construction of 3-D statistical deformation models of the brain using nonrigid registration. *IEEE Trans Med Imaging* **22**, 1014–1025.

Schmid H, O'Callaghan P, Nash MP, Lin W, Legrice IJ, Smaill BH, Young AA & Hunter PJ (2008). Myocardial material parameter estimation: a non-homogeneous finite element study from simple shear tests. *Biomech Model Mechanobiol* **7**, 161–173.

Scollan DF, Holmes A, Winslow R & Forder J (1998). Histological validation of myocardial microstructure obtained from diffusion tensor magnetic resonance imaging. *Am J Physiol Heart Circ Physiol* **44**, H2308–H2318.

Sermesant M, Forest C, Pennec X, Delingette H & Ayache N (2003). Deformable biomechanical models: application to 4D cardiac image analysis. *Med Image Anal* **7**, 475–488.

Sermesant M, Moireau P, Camara O, Sainte-Marie J, Andriantsimiavona R, Cimrman R, Hill DL, Chapelle D & Razavi R (2006). Cardiac function estimation from MRI using a heart model and data assimilation: advances and difficulties. *Med Image Anal* **10**, 642–656.

Sermesant M, Peyrat JM, Chinchapatnam P, Billet F, Mansi T, Rhode K, Delingette H, Razavi R & Ayache N (2008). Toward patient-specific myocardial models of the heart. *Heart Fail Clin* **4**, 289–301.

Sermesant M, Rhode K, Sanchez-Ortiz GI, Camara O, Andriantsimiavona R, Hegde S, Rueckert D, Lambiase P, Bucknall C, Rosenthal E, Delingette H, Hill DL, Ayache N & Razavi R (2005). Simulation of cardiac pathologies using an electromechanical biventricular model and XMR interventional imaging. *Med Image Anal* **9**, 467–480.

Setser RA, Bexell DG, O'Donnell TP, Stillman AE, Lieber ML, Schoenhagen P & White RD (2003). Quantitative assessment of myocardial scar in delayed enhancement magnetic resonance imaging. *JMRI* **18**, 434–441

Smith NP, Pullan AJ & Hunter PJ (2000). Generation of an anatomically based geometric coronary model. *Ann Biomed Eng* **28**, 14–25.

Smith NP, Pullan AJ & Hunter PJ (2002). An anatomically based model of coronary blood flow and myocardial mechanics. *SIAM J Applied Mathematics* **62**, 990–1018.

Sodickson DK (2000). Tailored SMASH image reconstructions for robust in vivo parallel MR imaging. *Magn Reson Med* **44**, 243–251.

Sodickson DK & Manning WJ (1997). Simultaneous acquisition of spatial harmonics (SMASH): fast imaging with radiofrequency coil arrays. *Magn Reson Med* **38**, 591–603.

Suinesiaputra A, Frangi AF, Kaandorp TAM, Lamb HJ, Bax JJ, Reiber JHC & Lelieveldt BPF (2009). Automated detection of regional wall motion abnormalities based on a statistical model applied to multi-slice short-axis cardiac MR images. *IEEE Trans Med Imaging*, in press.

Suinesiaputra A, Frangi AF, Uzumcu M, Reiber JHC & Lelieveldt BPF (2004). Extraction of myocardial contractility patterns from short-axes MR images using independent component analysis. In *Computer Vision Approaches to Medical Image Analysis (CVAMIA) and Mathematical Methods in Biomedical Image Analysis (MMBIA) Workshop*, ed. Sonka M, Kakadiaris I, Kybic J. Lecture Notes in Computer Science, **vol. 3117**, pp. 75–86, Springer Verlag, Berlin, Germany.

Sutton MG & Sharpe N (2000). Left ventricular remodeling after myocardial infarction: pathophysiology and therapy. *Circulation* **101**, 2981–2988.

Taguchi K & Aradate H (1998). Algorithm for image reconstruction in multi-slice helical CT. *Med Phys* **25**, 550–561.

ten Tusscher KHWJ, Noble D, Noble PJ & Panfilov AV (2004). A model for human ventricular tissue. *Am J Physiol Heart Circ Physiol* **286**, H1573–H1589.

ten Tusscher KHWJ & Panfilov AV (2006). Cell model for efficient simulation of wave propagation in human ventricular tissue under normal and pathological conditions. *Phys Med Biol* **51**, 6141–6156.

Tobon-Gomez C, Butakoff C, Sukno F, Aguade S, Moragas G & Frangi AF (2008). Automatic construction of 3D-ASM intensity models by simulating image acquisition: application to myocardial gated SPECT studies. *IEEE Trans Med Imaging* **27**, 1655–1667.

Trayanova NA (2006). Defibrillation of the heart: insights into mechanisms from modelling studies. *Exp Physiol* **91**, 323–337.

van Assen HC, Danilouchkine MG, Dirksen MS, Reiber JH & Lelieveldt BP (2008). A 3-D active shape model driven by fuzzy inference: application to cardiac CT and MR. *IEEE Trans Inf Technol Biomed* **12**, 595–605.

van Assen HC, Danilouchkine MG, Frangi AF, Ordás S, Westenberg JJM, Reiber JHC & Lelieveldt BPF (2006). SPASM: a 3D-ASM for segmentation of sparse and arbitrarily oriented cardiac MRI data. *Med Image Anal* **10**, 286–303.

Vigmond EJ, Clements C, McQueen DM & Peskin CS (2008*a*). Effect of bundle branch block on cardiac output: a whole heart simulation study. *Prog Biophys Mol Biol* **97**, 520–542.

Vigmond EJ, Weber dos Santos R, Prassl AJ, Deo M & Plank G (2008*b*). Solvers for the cardiac bidomain equations. *Prog Biophys Mol Biol* **96**, 3–18

von Berg J & Lorenz C (2007). A geometric model of the beating heart. *Methods Inf Med* **46**, 282–286.

Wagner A, Mahrholdt H, Holly TA, Elliot MD, Regenfus M, Parker M, Klocke FJ, Bonow RO, Kim RJ & Judd RM (2003). Contrast-enhanced MRI and routine single photon emission computed tomography. *Lancet* **361**, 374–381.

Wang VY, Lam HI, Ennis DB, Young AA & Nash MP (2008). Passive ventricular mechanics modelling using MRI structure and function. *MICCAI 2008*, LNCS 5242, **11**, 814–821.

Weiger M, Pruessmann KP & Boesiger P (2000). Cardiac real-time imaging using SENSE. SENSitivity Encoding scheme. *Magn Reson Med* **43**, 177–184.

Young AA & Axel L (1992). Three-dimensional motion and deformation of the heart wall: estimation with spatial modulation of magnetization – a model-based approach. *Radiology* **185**, 241–247.

Young AA, Cowan BR, Thrupp SF, Hedley WJ & Dell'Italia LJ (2000). Left ventricular mass and volume: fast calculation with guide-point modeling on MR images. *Radiology* **216**, 597–602.

Young AA, French BA, Yang Z, Cowan BR, Gilson WD, Berr SS, Kramer CM & Epstein FH (2006). Reperfused myocardial infarction in mice: 3D mapping of late gadolinium enhancement and strain. *J Cardiovasc Magn Reson* **8**, 685–692.

Young AA, Kraitchman DL, Dougherty L & Axel L (1995). Tracking and finite element analysis of stripe deformation in magnetic resonance tagging. *IEEE Trans Med Imaging* **14**, 413–421.

Young AA, Kramer CM, Ferrari VA, Axel L & Reichek N (1994). Three-dimensional left ventricular deformation in hypertrophic cardiomyopathy. *Circulation* **90**, 854–867.

Acknowledgements

A.A.Y. would like to acknowledge B. R. Cowan of the University of Auckland Center for Advanced MRI, C. G. Fonseca of the University of California Los Angeles, and funding from the Health Research Council of New Zealand and the National Institutes of Health (R01HL087773) USA. A.F.F. would like to acknowledge B. H. Bijnens, C. Butakoff, C. Hoogendoorn, S. Ordas, D. Romero, R. Sebastián, F. M. Sukno and C. Tobón-Gomez from his laboratory for some of the figures in this manuscript and for fruitful discussions. Funding from the European Commission (euHeart Project, www.euheart.eu) and the Centro para el Desarrollo Tecnológico Industrial from Spanish Ministry of Innovation and Science (CDTEAM Project, www.cdteam.org) are greatly acknowledged.